Characterization of Direct-Current Atmospheric-Pressure Discharges Useful for Ambient Desorption/Ionization Mass Spectrometry

Jacob T. Shelley, Joshua S. Wiley, George C. Y. Chan, Gregory D. Schilling, Steven J. Ray, and Gary M. Hieftje
Department of Chemistry, Indiana University, Bloomington, Indiana, USA

Two relatively new ambient ionization sources, direct analysis in real time (DART) and the flowing atmospheric-pressure afterglow (FAPA), use direct current, atmospheric-pressure discharges to produce reagent ions for the direct ionization of a sample. Although at a first glance these two sources appear similar, a fundamental study reveals otherwise. Specifically, DART was found to operate with a corona-to-glow transition (C-G) discharge whereas the FAPA was found to operate with a glow-to-arc transition (G-A) discharge. The characteristics of both discharges were evaluated on the basis of four factors: reagent-ion production, response to a model analyte (ferrocene), infrared (IR) thermography of the gas used for desorption and ionization, and spatial emission characteristics. The G-A discharge produced a greater abundance and a wider variety of reagent ions than the C-G discharge. In addition, the discharges yielded different adducts and signal strengths for ferrocene. It was also found that the gas exiting the discharge chamber reached a maximum of 235 °C and 55 °C for the G-A and C-G discharges, respectively. Finally, spatially resolved emission maps of both discharges showed clear differences for N_2^+ and O(I). These findings demonstrate that the discharges used by FAPA and DART are fundamentally different and should have different optimal applications for ambient desorption/ionization mass spectrometry (ADI-MS). (J Am Soc Mass Spectrom 2009, 20, 837–844) © 2009 Published by Elsevier Inc. on behalf of American Society for Mass Spectrometry

Direct-current (DC) discharges have been widely used for elemental analyses since they were first introduced for alloy characterization [1]. When DC discharges were coupled with mass spectrometry, the result was a very sensitive and powerful tool for elemental [1] and molecular analyses [2, 3]. Of the many electrical regimes of DC discharges, three forms have been found to have particular analytical merit: the arc, the glow, and the corona. Among these three types of discharges, the fundamental distinction is the operating current and voltage. The arc occurs at very high currents (hundreds of amperes) with a low voltage drop between electrodes (tens of volts). It also exhibits negative resistance; that is, the sustaining voltage drops as the current rises. The glow discharge (GD), which has conventionally been operated between 0.1 to 10 Torr, exists at much lower currents (tens of milliamperes) and a higher voltage drop (hundreds of volts). Lastly, the corona discharge operates with very low currents (a few microamperes) and a much higher voltage drop (several kilovolts).

Corona discharges find their most common analytical application in atmospheric pressure chemical ionization (APCI) [4, 5]. In conventional APCI, a corona discharge is formed by applying ~4 kV to a needle electrode in a selected atmosphere, to yield currents of ~5 μA. After a series of reactions [5], reagent ions are produced that can then ionize a sample. Protonated water clusters are typically observed because of the presence of water vapor in the air. Such protonated clusters promote proton transfer ionization, resulting in mass spectra containing mainly the protonated molecular ion (MH^+). However, a limitation of APCI sources is the relatively low flux of reagent ions they produce because of the low discharge current. This low flux often results in ion suppression caused by competitive ionization reactions when multiple analytes are present. To overcome this problem, APCI is usually coupled with a separation technique.

Conventional glow discharge ionization sources operate at reduced pressure, which often results in fragmentation of the analyte by impact from energetic electrons, and leads to more complicated mass spectra.

Address reprint requests to Dr. G. M. Hieftje, Department of Chemistry, Indiana University, 800 E. Kirkwood Avenue, Bloomington, IN 47405, USA). E-mail: hieftje@indiana.edu

1044-0305/09/$32.00
doi:10.1016/j.jasms.2008.12.020

Published online January 1, 2009
Received August 25, 2008
Revised December 19, 2008
Accepted December 20, 2008

In addition, special sample introduction systems must be devised to place the sample under vacuum conveniently. One way to overcome these obstacles is to operate the discharge at atmospheric pressure. However, when a DC discharge is operated at atmospheric pressure, some of its characteristics change dramatically, among them the current-voltage behavior [6].

Lubman et al. [7, 8] showed that an atmospheric-pressure glow discharge (APGD) can be used as an ionization source for molecular mass spectrometry. Lubman's source employed helium as the discharge gas and typically yielded a mass spectrum containing only a molecular ion peak (similar to APCI), making the spectra easy to interpret. However, his configuration required introduction of the sample into the discharge chamber, leading to memory effects, instabilities in the discharge, and sample-induced changes in the characteristics of the GD. Clearly, a source not requiring introduction of the sample into the discharge chamber would be desirable.

Recently, several ionization sources have been developed that separate the discharge from the sampling region [9–11]. By introducing the sample beyond the discharge chamber, the problems of discharge instability and memory effects have been overcome. These sources are commonly employed in the new field of ambient desorption/ionization mass spectrometry (ADI-MS) [12], which refers to an open-air ionization source that permits the direct ionization (and often desorption) of samples for mass spectrometry. One such ADI-MS source is direct analysis in real time (DART) [10]. Unfortunately, little has been reported about the fundamental characteristics of the discharge used in DART, but both a corona and a glow discharge have been claimed. Developed by JEOL USA Inc. (Peabody, MA), DART is often operated near −3 kV with currents up to 5 mA [10]. The discharge is typically formed in helium between a pin cathode and a grounded, disk anode. Two filter electrodes are placed beyond the discharge chamber to remove any charged species, resulting in predominantly helium metastables (He*) exiting the source. Additionally, the gas temperature is raised to ~300 °C by an auxiliary heater. Samples are introduced into the open-air sampling region, after the second filter electrode, for direct desorption/ionization. The interaction between He* and open air results in the production of reagent ions similar to those in APCI [5]. Thus, when an analyte is desorbed/ionized, the resulting mass spectrum consists mainly of the molecular ion.

Another ADI-MS source based on a DC discharge in helium has recently been developed and described by our laboratory [13–15]. This source, termed the flowing atmospheric pressure afterglow (FAPA) ionization source, operates by the formation of a true glow discharge in helium between a pin cathode and plate anode, with voltages between −400 and −500 V and operating currents of roughly 25 mA [13]. Although FAPA and DART might seem to be similar, a fundamental characterization of the two discharges is essential to understand them fully.

In the present study, the discharges used by DART and FAPA, a corona-to-glow (C-G) and a glow-to-arc (G-A) transitional discharge, respectively, were characterized on the basis of several criteria. Electrical characteristics of both the DART and FAPA discharge were initially used to classify each. The reagent ions produced, along with the mass spectra for ferrocene generated by both discharges were also compared. Thermal maps of the gas escaping the discharge cell of both sources were examined as well. Lastly, spatially resolved emission maps for O(I) and N_2^+ generated by both discharges were measured. Overall, it was found that the two kinds of discharge are fundamentally different, and might be best applied in dissimilar areas.

Experimental

Reagents

All reagents were analytical grade. High purity He (99.9999% ultra high purity helium; Airgas, Radnor, PA) was used as the discharge gas in all experiments. Ferrocene was purchased from Sigma-Aldrich (St. Louis, MO) and used as a model compound because of its high vapor pressure, which simplified sample introduction.

Instrumentation

An atmospheric pressure discharge in helium was formed in an airtight cell with a quartz body (cf. Figure 1). The discharge was established between a stainless steel pin (cathode) and a brass plate (anode) with a discharge gap of ~7 mm. A small hole (~1 mm dia.) in the center of the brass plate allowed species generated in the discharge to flow into the open atmosphere. To compensate for the inherent negative dynamic resistance of atmospheric pressure discharges, a ballast resistance was placed in series with the cathode. Ultimately, this ballast resistance limits the obtainable discharge current. A negative voltage was applied to the cathode with a high-voltage, DC power supply (model

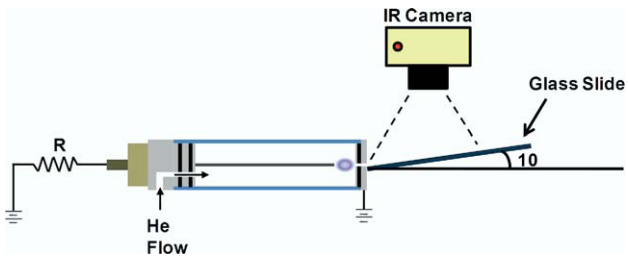

Figure 1. Diagram of the quartz cell used for forming the different discharges in helium in the configuration used for obtaining thermographic images of the gas exiting the cell. The slide was placed nearly parallel to the gas flow to measure the greybody emission from the glass slide.

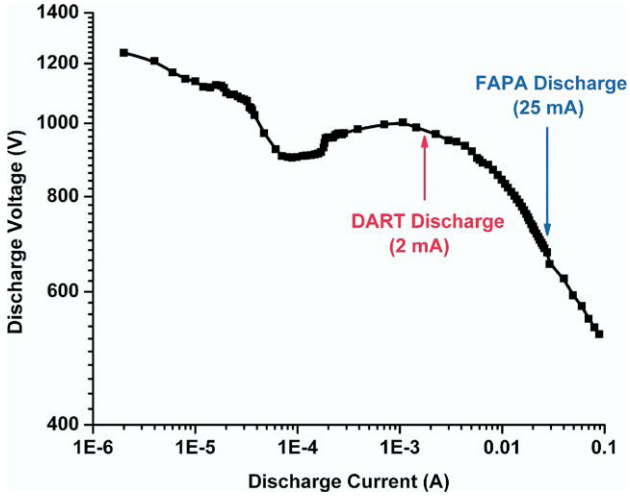

Figure 2. Characteristic current-voltage curve for atmospheric-pressure, DC discharges formed in helium. Cell configuration was a pin-to-plate geometry with a gap of ~7 mm (cf. Figure 1).

BRC-5-400R; Universal Voltronics Corp., Mt. Kisco, NY), with helium being supplied to the cell by a mass flow controller (MKS Instruments, Andover, MA).

The C-G and G-A discharges (see section on discharge classification below) were formed in the same discharge chamber, but under different operating conditions. For this chamber, the current-voltage behavior is illustrated in Figure 2. The C-G (DART-like) discharge, with current-voltage conditions labeled with a red arrow in Figure 2, was sustained by using a ballast resistance of 1 MΩ and applying a voltage of −3 kV to the pin, resulting in currents of less than 3 mA. It is important to note that the additional electrodes and heater, which are used in the commercial DART, were excluded to investigate fundamental properties of the discharge. The G-A (FAPA-like) discharge, labeled with a blue arrow in Figure 2, was operated with a ballast resistance of 1.5 kΩ and operated at 25 mA and −450 V. Helium metastables, along with other discharge products, exit the cell through the small hole in the anode, and ionize N_2 and H_2O in open air, resulting in the production of reagent ions [4, 16, 17]. The voltage of the anode was adjusted with a low-voltage DC power supply (model 6299A; Hewlett Packard, Palo Alto, CA) to maintain a field-free sampling region between the discharge cell and the mass spectrometer interface when mass spectrometry was performed. The cell was mounted on a locally built three-dimensional translation stage for alignment with the sampling orifice of the mass spectrometer.

Mass Spectrometer

Ions were detected by a modified LECO Renaissance (LECO Corp. St. Joseph, MI) inductively coupled plasma (ICP) time-of-flight mass spectrometer (TOFMS), with the ICP source disabled and replaced with the discharge cell. Modifications to the MS have already been described [13], but a brief overview is given here. The original sampling cone was machined flat to yield a stainless-steel sampling plate. In addition, a 3-mm diameter copper ring electrode, serving as an ion lens, was added between the skimmer and the front plate to better focus and guide the incoming ion beam. The voltage of the ion lens was independently controlled with a low voltage power supply (model 6207B; Hewlett Packard-Harrison Division, Berkeley Heights, NJ). To overcome a higher first-stage pressure caused by the introduction of helium, an additional roughing pump was added to the first stage. An integration time of 0.5 s was used in all MS experiments.

IR Thermography

Thermal spatial patterns of the gas exiting the discharge cell were taken for the C-G and G-A discharges by means of a Fluke Ti40 IR FlexCam (Everett, WA). A glass microscope slide was placed nearly parallel (~10°) to the gas flow, but slightly angled so the slide was in the path of the gas stream issuing from the cell (cf. Figure 1). The reason for this arrangement is that the gas leaving the discharge chamber does not behave as either a blackbody or greybody. In this experiment, the gas transfers its heat to the glass slide, the greybody emission of which can be detected with the camera. The poor thermal conductivity of glass (1.1 $W/m \cdot K$) along with its high emissivity (0.92) made it a good choice for spatially resolved, greybody emission measurements. The emissivity of the glass was taken into consideration to obtain accurate temperatures.

Optical Spectroscopic Measurements

Longitudinally resolved (side-on) spectroscopic measurements of both discharges were obtained by mounting the quartz discharge cell in place of the ICP ordinarily used in a commercial emission spectrometer (ACTIVA; Horiba-Jobin Yvon, Longjumeau, France). The discharge cell was mounted on a movable platform for proper alignment of the discharge with the entrance slit. The spectral resolution of this instrument is between 8 and 16 pm, depending on the wavelength region being employed. The ACTIVA spectrometer has the advantage of simultaneously providing wavelength and spatial information with a spatial resolution of ~200 μm. To achieve this spatial resolution, a cylindrical lens was placed in the entrance optics between the front mirror and the entrance slit. With this modification, the spectrometer also has the ability to image lengths greater than 20 mm, which allowed full spectral imaging of the electrodes and the discharge. Species of interest included N_2^+ and O(I) at emission wavelengths of 309.40 and 777.19 nm, respectively. Although ultra-high purity helium was used, these impurities apparent from the emission spectrum arise from the gas transfer

lines. As previously noted [13], the impurities could be removed by thorough baking of the transfer lines and gas purification immediately before the discharge chamber. However, this extensive procedure was deemed unnecessary in this initial study.

Results and Discussion

Discharge Classification

Figure 2 demonstrates the current-voltage (i-V) plot for an atmospheric-pressure DC discharge operated in a pin-to-plate geometry, with helium as the discharge gas. This i-V curve differs greatly from that for a reduced-pressure discharge. The transitions between the different discharge regimes become less pronounced, making discharge classification difficult. In addition, the pin-to-plate geometry introduces a corona realm. The red arrow in Figure 2 identifies where the discharge used by DART operates [18–20], in a C-G transitional zone. The FAPA discharge, found in the G-A transitional regime, is labeled on the current-voltage curve of Figure 2 with the blue arrow.

Photographs of the C-G and G-A discharges are shown in Figure 3a and 3b, respectively. The exposure time for the photograph in Figure 3b is four times shorter than that required for Figure 3a, indicating that the G-A discharge is much brighter. In addition, only the tip of the cathode glows (negative glow region) in the C-G discharge, whereas the negative glow extends further down the cathode with the G-A discharge. This behavior is expected; in a "normal" glow discharge, the area of the negative glow is proportional to the supplied current. Another feature is the extended and brighter positive column found with the G-A discharge (Figure 3b) compared with the very dim positive column for the C-G discharge (Figure 3a). Atmospheric pressure glow discharges typically have a fairly bright positive column that fills most of the gap between the anode and cathode, as was observed with the G-A discharge. Corona discharges, in contrast, usually do not have a visible positive column; thus, the presence of a weak positive column with the C-G discharge suggests that it operates between the corona and the glow discharge regimes.

Interesting also are the standing striations in the positive column of the G-A discharge. Although these striations have been observed only with certain cell configurations and do not seem to affect the performance of the source, they are useful in characterizing the discharge. Such standing striations represent local maxima of current density. Because nearly all of the current density in a corona discharge resides at or near the tip of the electrode, corona discharges cannot exhibit such striations. For this reason, the striations do not appear in the C-G discharge.

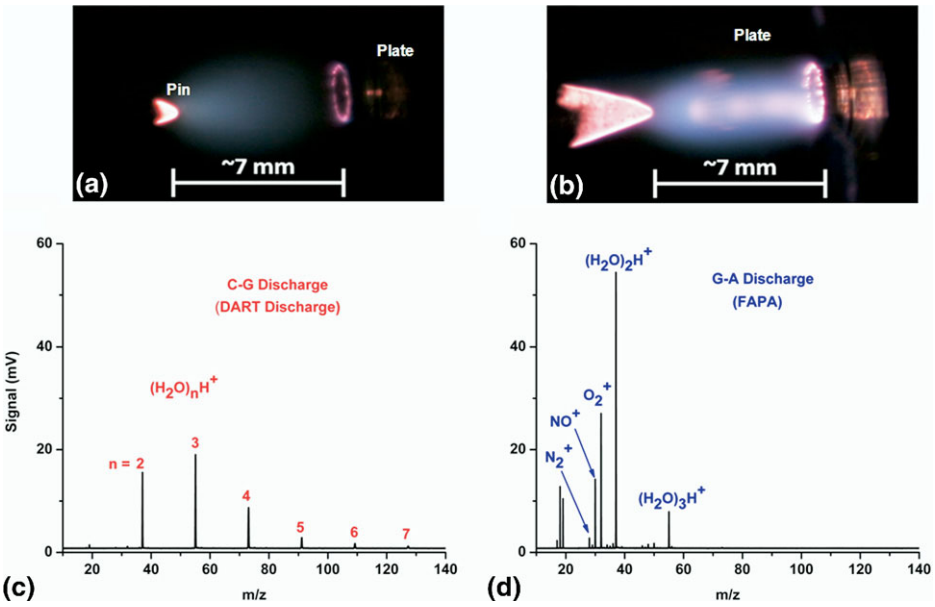

Figure 3. (**a**) C-G discharge operated at a current of 2 mA and photographed with a 1/15 s exposure time. The strongest emission occurs at the tip of the pin cathode (left), with a very faint, diffuse positive column, similar to the pattern expected from a corona discharge. (**b**) G-A discharge operated at a current of 25 mA and photographed with a 1/60 s exposure time. The negative glow extends farther down the cathode tip and there is a better confined, brighter positive column, just as in a conventional glow discharge. The standing striations in the positive column were present only in certain cell configurations and have not been found to affect the performance of the source. (**c**) and (**d**) Background mass spectra from the C-G and G-A discharges, respectively. The main features with the C-G discharge are protonated water clusters, whereas the G-A discharge contains additional charge-transfer reagent ions such as O_2^+, and fewer higher-order water clusters.

Table 1. Operating conditions for the C-G and G-A discharges optimized for generating the strongest $(H_2O)_2H^+$ signal

	C-G discharge	G-A discharge
Cathode voltage, current	−3000 V, ~2 mA	−500 V, 25 mA
Anode voltage	110 V	70 V
MS front-plate voltage	80 V	50 V
He flow	~1.5 L/min	~1 L/min
Ballast resistance	1 MΩ	1.5 kΩ

Reagent Ions

All discharge and MS parameters were tuned to maximize the signal from $(H_2O)_2H^+$ for both discharges. The strong signal for $(H_2O)_2H^+$ made it an effective reagent ion for optimization because of its high abundance in the mass spectrum of both discharges (Figure 3c and d) and its extremely high gas-phase acidity. This trait promotes efficient proton-transfer ionization even for analytes with low gas-phase basicity, yielding an MH^+ molecular ion. The parameters that affected the reagent-ion signal included the voltage on the front plate of the mass spectrometer, the anode voltage, and the He flow. The resulting optimal operating conditions are given in Table 1.

To better understand the C-G and G-A discharges, it is useful to determine the relative abundance and type of reagent ions that are produced by each. The presence of protonated species, particularly protonated water clusters, suggests the likelihood of a proton-transfer ionization mechanism in which the proton is transferred from the reagent ion to the sample species. Another type of ionization that might take place is charge-transfer, in which a positively charged reagent ion steals an electron from the sample species, to become neutral while the sample species assumes a positive charge. For either mechanism, the greater the abundance of ions available to transfer their charge, the higher the ionization probability and the less likely that competitive ionization will distort observed spectra.

The reagent-ion spectrum from the C-G discharge, shown in Figure 3c, contains mainly protonated water clusters, which foster a proton-transfer ionization mechanism. Virtually no ions for charge-transfer ionization, such as N_2^+, NO^+, or O_2^+, were detected with the C-G discharge. The likely reason for this observation is that the lower power C-G discharge generates a lower abundance of He* and other species necessary for producing the charge-transfer reagent ions. The reagent ion spectrum from the G-A discharge was substantially different (Figure 3d). In addition to protonated water clusters, the G-A discharge produced a significant amount of NO^+, O_2^+, and N_2^+. These three ions have been shown to play a role in charge-transfer ionization [21], which would result in the formation of molecular ions, $M^{+\cdot}$. Additionally, the mass spectrum from the G-A discharge exhibits a stronger reagent ion signal than does the C-G discharge. Moreover, the C-G discharge produces a greater abundance of higher-order water clusters, which have lower gas-phase acidity and yield less efficient ionization than lower-order protonated clusters. Therefore, the G-A discharge would be expected to offer a wider range of ionization capabilities, in addition to being less affected by competitive ionization of multiple analytes.

Ferrocene Determination

Ferrocene was introduced into the sampling region of each discharge by passing helium, at ~120 mL/min, across a few crystals of ferrocene placed in a gas-tight flask and through a narrow glass tube (~300 μm i.d.). The tube was held in the sampling region by means of a micropositioner to optimize the ferrocene signal. The G-A discharge was first ignited, thereby ionizing the vapor-phase ferrocene, which was then detected with the TOFMS. The signal trace for the $M^{+\cdot}$ of ferrocene (m/z = 186) was recorded for 3 min. The discharge was then extinguished, and the current-voltage conditions were changed to those of the optimized C-G discharge. The C-G discharge was then ignited and the signal for the M^+ from ferrocene again monitored for several more minutes. This time-trace for m/z 186 is given in Figure 4a. It is important to note that while these

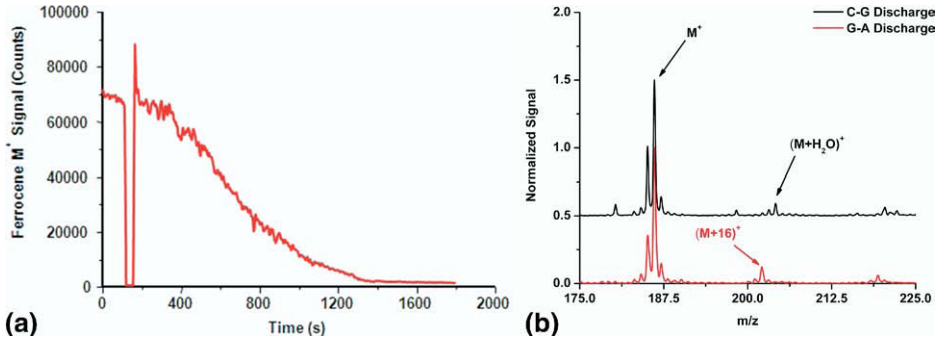

Figure 4. (**a**) Time trace for the molecular ion (M^+) of ferrocene (m/z = 186) with the G-A discharge as the initial ionization source. After two minutes, the source was turned off and switched to a C-G discharge. The signal then decayed over time to ~2% of the original level. See text for discussion. (**b**) Normalized mass spectra of ferrocene obtained with a G-A discharge (black), and a C-G discharge (red) as ionization sources. The spectra are vertically offset from each other for visualization.

sources typically ionize through proton transfer, ferrocene has a much lower ionization energy than gas-phase basicity, resulting in mainly the molecular ion [22].

While the G-A discharge was running, there was a strong signal (~70,000 counts) for the M^+ of ferrocene. When the discharge was turned off, the signal went to zero, and then returned initially to ~70,000 counts when the C-G discharge was ignited. However, the subsequent signal decayed gradually to roughly 2% of its original strength. To verify that the signal decay was not due to a loss of ferrocene, the G-A discharge was later reignited and the signal returned to approximately its original level (~70,000 counts; data not shown). The gradual decay in signal during the initial C-G "on" period is believed to be related to discharge stabilization and slow cooling of the discharge cell. Although the cell temperature would not affect the ferrocene desorption process because the analyte is in the vapor phase before reaching the sampling region, it can alter the concentration and type of reagent ions that are produced. It was found that switching to the C-G discharge resulted in ion signal decay for low-order water clusters and charge-transfer ions, resulting in a drop in ionization efficiency. Additionally, the signal for higher-order clusters (n = 3 or 4) gradually rose over time (data not shown), which implies that the lower gas temperature resulted in condensation of water clusters. However, the exact reason for the decay in charge-transfer ion signal is not yet known.

Spectra of ferrocene obtained with the C-G and the G-A discharges are given in Figure 4b. The G-A discharge produced, in addition to the molecular ion, an adduct with a mass shifted higher by 16 u, thought to be an addition of oxygen by the reaction of radical, atomic oxygen with the aromatic ring of ferrocene [23]. The only adduct observed with the C-G discharge was an addition of 18 u, attributed to water. Both of these spectra match well with those published for typical APCI sources [22] and the commercial DART source [24].

IR Thermography

For a source to be attractive, practically, for ADI-MS, it must not only efficiently ionize, but also desorb analytes. Because it is believed that the major mechanism of desorption in APGD-based ADI-MS sources is thermal [9], it is useful to measure the temperature of the gas exiting the discharge cell. Furthermore, a full thermographic map of the gas could yield important information about optimal sample positioning for desorption/ionization.

IR thermography of the C-G and G-A discharges was performed by measuring the blackbody emission from a glass microscope slide that was in contact with the gas stream. Temperature profiles for the C-G and G-A discharges under optimal conditions are given in Figure 5a and b, respectively. These images reveal that the gas issuing from the G-A discharge was much hotter (maximum temperature ~235 °C) than that from the C-G discharge (maximum temperature ~55 °C). This difference in temperature is due to a higher current density in the G-A discharge, stemming from larger operating currents, than in the C-G discharge. The higher temperature of the G-A discharge should yield more efficient desorption, and thus more sensitive detection, of molecules with lower vapor pressures. This fact also likely explains why an auxiliary heater is employed with the DART source, which utilizes a C-G discharge. Otherwise, many solid samples would not be efficiently desorbed, resulting in low detection efficiency and sensitivity.

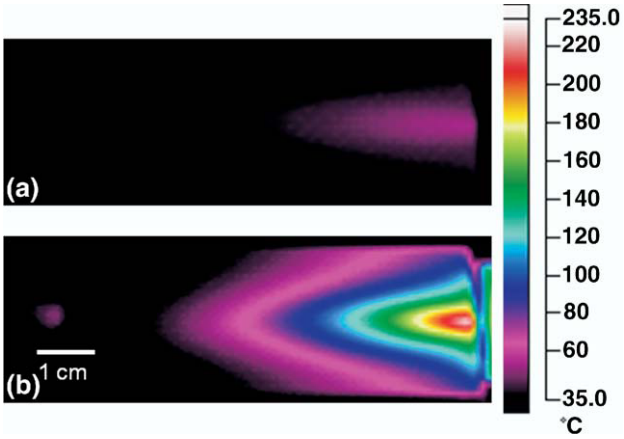

Figure 5. Thermographic map of the gas stream issuing from the C-G discharge (**a**) and the G-A discharge (**b**) under optimal conditions and on the same false-color temperature scale (right). The C-G discharge attains a maximum temperature of only ~55 °C, whereas the G-A discharge reaches ~235 °C.

Optical Emission

To better understand the two discharges, the spatial distribution of selected emission features, known to exist in the spectrum [13], was obtained. Spatially resolved emission maps for N_2^+ (at 391.4 nm) and O(I) (at 777.19 nm) are shown in Figure 6a and b, respectively. It should be emphasized that both features arise from contaminants in the He supply, so would be expected to be weak. For both spectral features, and both discharges, there are distinct emission maxima at the pin (cathode) and plate (anode). The peak at the cathode is due to the strong emission from the negative glow. Nearly all of the emission [~95% in the case of O(I)], and consequently current density, of the C-G discharge is restricted to the very tip of the pin. In contrast, the emission from the G-A discharge was distributed along the length of the pin (~2 mm) and the throughout the positive column. At atmospheric pressure, the positive column occupies much of the discharge region in glow discharges [13], whereas corona discharges do not exhibit a strong positive column. In the maps of the two discharges, emission from N_2^+ and O can clearly be seen in the positive column of the G-A discharge, but not with the C-G discharge even at long

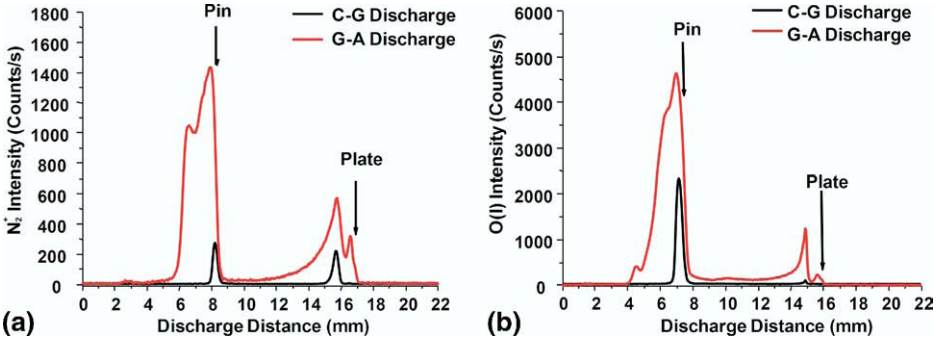

Figure 6. (**a**) Spatially resolved optical emission from N_2^+ for C-G and G-A discharges. (**b**) Optical emission from O(I) for the C-G and G-A discharges. These emission lines come from trace gas impurities in the transfer lines. The spatial emission plots demonstrate that the C-G discharge is confined to the tip of the pin with little or no positive column, which is indicative of a corona discharge.

exposure times (60 s). These emission patterns indicate that the G-A discharge is a true glow and should be capable of generating a large flux of excited species.

Conclusion

The C-G and G-A discharges, used by DART and FAPA respectively, have been examined in some detail. They have been shown to produce different types and amounts of reagent ions. Additionally, the C-G discharge produces a water adduct with the M^+ of ferrocene, whereas an oxygen adduct was seen with the G-A discharge. Infrared thermography of the gas exiting the discharge cell revealed that the plume from the G-A discharge is much hotter than from the C-G discharge. This temperature difference suggests why an external heater is needed for direct analyses with the DART source. The relative peak heights at the anode and cathode for emission from atomic oxygen and N_2^+ suggests that the C-G discharge is closer to a corona discharge and the G-A closer to a GD. This study demonstrates that the two discharges are fundamentally different and should offer individual advantages. However, a direct comparison of the desorption/ionization capabilities of these sources is essential and will be the basis of a subsequent study. Additionally, a fundamental examination and comparison of all ADI-MS sources, including desorption electrospray ionization (DESI), FAPA, and DART, is needed. Parameters of interest include sensitivity, range of detectable analytes, stability, and matrix-effect ion suppression. Not only would this study provide users with information for choosing the proper source for a given application, but it is essential to the progression and widespread adoption of the method.

References

1. Kay, E.; Coburn, J. Quantitative Elemental Analysis of Thin Solid Layers by Glow Discharge Mass Spectrometry. *Electronica y Fisica Aplicada* **1974,** *17*(1/2), 246–246.
2. Carazzato, D.; Bertrand, M. J. Characterization of a Glow Discharge Ion Source for the Mass Spectrometric Analysis of Organic Compounds. *J. Am. Soc. Mass Spectrom.* **1994,** *5*(4), 305–315.
3. Mason, R.; Milton, D. Glow Discharge Mass Spectrometry of Some Organic Compounds. *Int. J. Mass Spectrom. Ion Processes* **1989,** *91*(2), 209–25.
4. Horning, E. C.; Carroll, D. I.; Dzidic, I.; Haegele, K. D.; Horning, M. G.; Stillwell, R. N. Atmospheric Pressure Ionization (API) Mass Spectrometry. Solvent-Mediated Ionization of Samples Introduced in Solution and in a Liquid Chromatograph Effluent Stream. *J. Chromatogr. Sci.* **1974,** *12*(11), 725–9.
5. Horning, E. C.; Horning, M. G.; Carroll, D. I.; Dzidic, I.; Stillwell, R. N. New Picogram Detection System Based on a Mass Spectrometer with an External Ionization Source at Atmospheric Pressure. *Anal. Chem.* **1973,** *45*(6), 936–43.
6. Staack, D.; Farouk, B.; Gutsol, A.; Fridman, A. Characterization of a D.C. Atmospheric Pressure Normal Glow Discharge. *Plasma Sources Sci. Technol.* **2005,** *14*(4), 700–711.
7. Sofer, I.; Zhu, J.; Lee, H. S.; Antos, W.; Lubman, D. M. An Atmospheric-Pressure Glow Discharge Ionization Source. *Appl. Spectrosc.* **1990,** *44*(8), 1391–1398.
8. Zhao, J.; Zhu, J.; Lubman, D. M. Liquid Sample Injection Using an Atmospheric Pressure Direct Current Glow Discharge Ionization Source. *Anal. Chem.* **1992,** *64*(13), 1426–33.
9. Venter, A.; Nefliu, M.; Cooks, R. G. Ambient Desorption Ionization Mass Spectrometry. *Trac-Trends Anal. Chem.* **2008,** *27*(4), 284–290.
10. Cody, R. B.; Laramee, J. A.; Durst, H. D. Versatile New Ion Source for the Analysis of Materials in Open Air under Ambient Conditions. *Anal. Chem.* **2005,** *77*(8), 2297–2302.
11. McEwen, C. N.; McKay, R. G.; Larsen, B. S. Analysis of Solids, Liquids, and Biological Tissues Using Solids Probe Introduction at Atmospheric Pressure on Commercial LC/MS Instruments. *Anal. Chem.* **2005,** *77*(23), 7826–7831.
12. Takats, Z.; Wiseman, J. M.; Gologan, B.; Cooks, R. G. Mass Spectrometry Sampling under Ambient Conditions with Desorption Electrospray Ionization. *Science* **2004,** *306*(5695), 471–473.
13. Andrade, F. J.; Wetzel, W. C.; Chan, G. C. Y.; Webb, M. R.; Gamez, G.; Ray, S. J.; Hieftje, G. M. A New, Versatile, Direct-Current Helium Atmospheric-Pressure Glow Discharge. *J. Anal. At. Spectrom.* **2006,** *21*(11), 1175–1184.
14. Andrade, F. J.; Shelley, J. T.; Wetzel, W. C.; Webb, M. R.; Gamez, G.; Ray, S. J.; Hieftje, G. M. Atmospheric Pressure Chemical Ionization Source. 1. Ionization of Compounds in the Gas Phase. *Anal. Chem.* **2008,** *80*(8), 2646–2653.
15. Andrade, F. J.; Shelley, J. T.; Wetzel, W. C.; Webb, M. R.; Gamez, G.; Ray, S. J.; Hieftje, G. M. Atmospheric Pressure Chemical Ionization Source. 2. Desorption-Ionization for the Direct Analysis of Solid Compounds. *Anal. Chem.* **2008,** *80,* 2654–2663.
16. Dzidic, I.; Carroll, D. I.; Stillwell, R. N.; Horning, E. C. Comparison of Positive-Ions Formed in Nickel-63 and Corona Discharge Ion Sources Using Nitrogen, Argon, Isobutane, Ammonia, and Nitric-Oxide as Reagents in Atmospheric-Pressure Ionization Mass-Spectrometry. *Anal. Chem.* **1976,** *48*(12), 1763–1768.
17. Kambara, H.; Mitsui, Y.; Kanomata, I. Identification of Clusters Produced in an Atmospheric-Pressure Ionization Process by a Collisional Dissociation Method. *Anal. Chem.* **1979,** *51*(9), 1447–1452.
18. Laramee, J. A., Cody, R. B. Method for Atmospheric Pressure Analyte Ionization. U.S. Patent 7112785 B2, 2006.
19. Laramee, J. A.; Durst, H. D.; Cody, R. B.; Nilles, J. M. Direct Analysis in Real Time (Dart): Chemical Agent Data and Background Physics, *Abstracts of Papers of the American Chemical Society* **230** (2005), U313.

20. Kpegba, K.; Spadaro, T.; Cody, R. B.; Nesnas, N.; Olson, J. A. Analysis of Self-Assembled Monolayers on Gold Surfaces Using Direct Analysis in Real Time Mass Spectrometry. *Anal. Chem.* **2007,** *79*(14), 5479–5483.
21. Einolf, N.; Munson, B. High Pressure Charge Exchange Mass Spectrometry. *Int. J. Mass Spectrom. Ion Phys.* **1972,** *9*(2), 141–160.
22. Macha, S. F.; McCarley, T. D.; Limbach, P. A. Influence of Ionization Energy on Charge-Transfer Ionization in Matrix-Assisted Laser Desorption/Ionization Mass Spectrometry. *Anal. Chim. Acta* **1999,** *97*(1/3), 235–245.
23. Ascenzi, D.; Franceschi, P.; Guella, G.; Tosi, P. Phenol Production in Benzene/Air Plasmas at Atmospheric Pressure. Role of Radical and Ionic Routes. *J. Phys. Chem. A* **2006,** *110*(25), 7841–7847.
24. Direct Analysis of Organometallic Compounds. In *DART Applications Notebook*, 4th ed.; JEOL Inc.: 2008; p 11.